REDUNDANT MANIPULATOR SELF-MOTION TOPOLOGY UNDER JOINT LIMITS WITH AN 8-DOF CASE STUDY

CARLOS L. LÜCK[1]
cluck@pollux.usc.edu

Department of Electrical Engineering - Systems[1]
University of Southern California
Los Angeles, CA .90089 -0781

SUKHAN LEE[1,2]
shlee@telerobotics.jpl.nasa.gov

Jet Propulsion Laboratory[2]
California *Institute of Technology*
Pasadena, CA 91109

Abstract: This paper investigates the topology of self-motion manifolds for serial redundant manipulators with revolute joints in the presence of joint limits. It is known that the preimages of singular taskpoints divide the configuration space into regions where self-llmtioll manifolds are homotopic. Initially, we describe how self-motion manifolds rupture as we move from one region 10 the next. The influence of joint limits on those topologies is investigated next. This analysis led to the discovery of the semi-singularity, a new type of singularity introduced by the presence of joint limits in redundant manipulators. A 3-DOF planar robot is used to illustrate the phenomena and a case study explores the concepts in more detail. This is an important analysis for global redundancy resolution and path planning because it describes the connectivity as well as the general for In of self-llolioli manifolds.

1 Introduction

An important aspect in the study of redundant manipulators is the issue of self-rllotion. A redundant manipulator generates infinite joint configurations for a given end-effector position. Those configurations can be described by a finite set of manifolds in the configuration space. They are called self-lnotiorl manifolds because the end-effector remains motionless as we reconfigure the arm along those manifolds.

Considering forward kinematics as the map:

$$\mathcal{F}(\theta) = x, \tag{1}$$

where $\theta \in \mathcal{C}$, the configuration space, and $x \in \mathcal{W}$, the work space, we describe inverse kinematics as the premap:

$$\mathcal{F}^{-1}(x) = \mathcal{M}(x), \tag{2}$$

where M is a collection of manifolds in the configuration space representing all inverse maps of the work space position x. [3] presents a good introduction to this issue and in order to avoid multiple notation we will preserve most of the terms defined there.

Based on the analysis of self motion manifold topologies, the configuration space is divided into several regions called c-bundles. Self-motion manifolds within a c-bundle are homotopic (see Definition 1), representing a homotopy class. The forward map of a c- bundle is a w-street, a region in the work space. Since inverse kinematics produces a collection of manifolds, the preimage of a w-sheet is a collection of c-bundles. C-bundles are separated by co-regular surfaces. A co-regular surface is formally defined as:

$$CS = \mathrm{F}\text{-}''(\mathrm{Y}''(\mathcal{S})) \tag{3}$$

where $\mathcal{S}$ is a manifold of singular configurations. $\mathcal{F}(\mathcal{S})$ is referred to in[3] as a critical value manifold arid in [11] as a jacobian surface. It is important, however, that $\mathcal{F}(\mathcal{S})$ be interior to the work space. Boundary singularities do not generate co-regular surfaces in general because they do not separate between reachable regions in the work space. 'There is one exception to that, however, and we will explore it in the case study.

This analysis in terms of manifold maps is useful for global path planning and optimization. It allows us to determine how to associate regions in the work space to regions in the configuration space and how to connect them as a certain task is to be performed. Furthermore, the connectivity and topology of self-motion manifolds is necessary for an effective global redundancy resolution strategy.

The main objective of this paper is to describe how joint limits affect self-r)mtion topologies, hut initially we present a discussion 011 what happens to the manifolds as we cross a co-regular surface.

The paper is organized as follows. In the next section we prove a theorem based on a variation of the classic definition of homotopy. in section 3, we describe the self-motion topology as we cross a co regular surface. The influence of joint limits is discussed in section 4. We introduce in section 5 a new type of singularity. Section 6 analyses the 8-DOF AA1 Arm as a case study. Section 7 is a summary and conclusion.

2 Preliminaries

Given the following definition [7],

Definition 1 *Two maps, $f_0 : X \to Y$ and $f_1 : X \to Y$ are homotopic if there is a smooth map, $F : X \times I \to Y$, I being the interval [0,1], such that $F(x,0) = f_0(x)$ and $F(x,1) = f_1(x)$,* i.e. *f_0 can be smoothly deformed to f_1.*

it is straightforward to prove that manifolds within a c-bundle are homotopic. This is done by taking F as the manifold inverse kinematics along a work space path which is interior to the corresponding w-sheet.

However, not much can be said about manifolds from different c-bundles. They are heterotopic (non-homotopic) in general but there are some cases where a smooth function connecting them can be found. 'This information, however, is of little use if such function dots not reflect the manipulator kinematics. We introduce a variation of the definition above as follows:

Definition 2 *Two maps are k-homotopic if they are homotopic under the manipulator kinematics,* i.e. *F is driven by the given manipulator* inverse *kinematics: $F(x,i) = \mathcal{M}(x(i))$, where $x(i)$ is an end-effector smooth trajectory.*

Based on this definition, we can state the following theorem:

Theorem 1 *Manifolds from different c-bundles are k-heterotopic.*

Proof: Any Continuous path connecting manifolds from different c-bundles rnrrst cross at least onc co-regular surface, which contains a singular point. Therefore, the manifold deformation

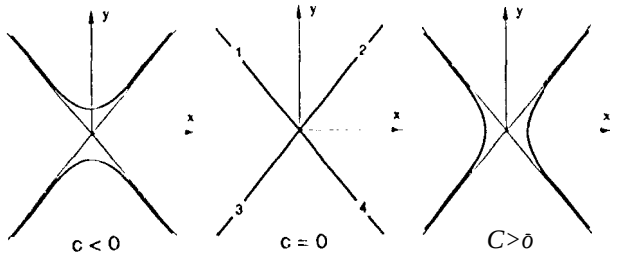

Figure 1: The Hyperbola $x^2 - y^2 = c$ as c crosses zero.

function 1", which is driven by inverse kinematics, can not be smooth.

Notice that, since inverse kinematics is the driving function, it is appropriate to consider a k-homotopy clam as the class of collections of *manifolds*. This class describes a collection of c-bundles as the premap of a single w-sheet.

3 Crossing Co-Regular Surfaces

At a singular point, the dimension of the self-)llotion is locally increased by the corresponding number of lost degrees of freedom. This fact is easily observed by analyzing the jacobian matrix. Any dimensional clccl'case in the range space is followed by a dimensional increase in the null space, since tbcy always add up to the dimension of the domain [9].

$$\dot{x} = J\dot{\theta}, \quad \mathrm{rk}(J) + \dim(\mathcal{N}) = n. \tag{4}$$

The local dimensional increase of the null space is observed in the configuration space of onc-degree-of-lcdurJdaJLcy manipulators as the intersection of two self-motion curves. This very aspect is the reason for not Considering a self-motion curve containing a singular point as a manifold in classical terms.

It is important to note, however, that self-l[lotiorls are restricted to those curves joined at the singular point. In other words, velocities can be generated along 2 different directions, but not along an arbitrary linear combination of those 2 directions as the jacobian analysis may suggest.

W c can easily extend this concept for multiple degrees of redundancy, but this phenomena is best visualized in terms of curves rather than surfaces or multidimensional primitives.

This section describes how those 2 curves split as wc move from one w-sheet to the next. At the neighborhood of an interior singularity, the self-rnotion manifolds are shaped as branches of a hyperbola:

$$x^2 - y^2 = c \tag{5}$$

with c < 0 in onc side, c > 0 in the other side and c = O at the jacobian sulfate. This transition justifies the topology change between neighboring k-homotopy classes. If wc label the 4 branches emerging from the singular point as 1, 2, 3 and 4 according to Figure 1, wc will scc the connections 1-2, 3-4 when c <0 and 1-3, 2-4 when c >0.

What happens outside this sufficiently small neighborhood is a global property and, as such, depends on particular arm classes, geometries and constraints. At the singularity and its immediate neighborhood, however, the hyperbolic pattern dominates. It is also important to note that Figure 1 is just a diffeomorphic representation of the phenomena. The actual self-n]otiorr curves arc

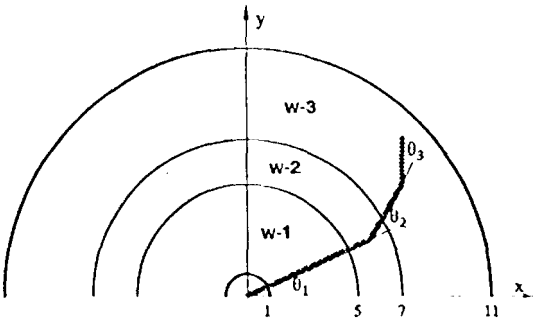

Figure 2: Planar Arm Work Space (top semi-disk shown only)

embedded in the configuration space which is multidimensional and not necessarily coplanar.

3.1 Example

Consider the link lengths $l_1 = 6$, $l_2 = 3$ and $l_3 = 2$ in the planar manipulator shown in Figure 2.

The jacobian surfaces shown at the polar radius $\rho = 5$ and 7 divide the work space into 3 w-sheets. W-sheets 1 and 3 arc premapped into a single region each in the configuration space (c-bundles 1 and 3 respectively) as show in Figure 3, and the self-motion manifolds in those regions are diffeomorphic to a circle (Figure *4).*

\V-sheet *2,* however, is premapped into a pair of regions in the configuration space (c-bundles 2a and 2b) and the self-nlotiml manifolds arc diffeomorphic to a pair of circles (there is an identification between points *360°* apart).

Bundles marked with one or more primes (') arc repetitions of the same pattern onc revolution apart and should be considered as the same bundle when there are no joint limits. This situation will change if joint limits are present, as wc will explore in the next section. Notice also that, for simplicity, the configuration space is represented by its projection onto the $\theta_2\theta_3$ plane. Due to the invariance of the patterns with respect to the polar angle of the end-effector, the third dimension is easily obtained by sweeping the curves with respect to the θ_1 axis.

Figure *5 shows* the connectivity among the various bundles.

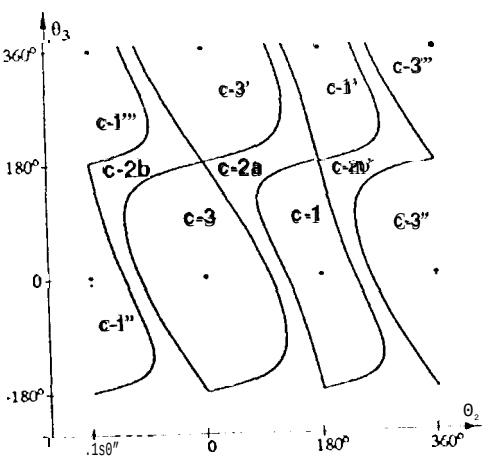

Figure 3: Planar Arm Configuration Space.

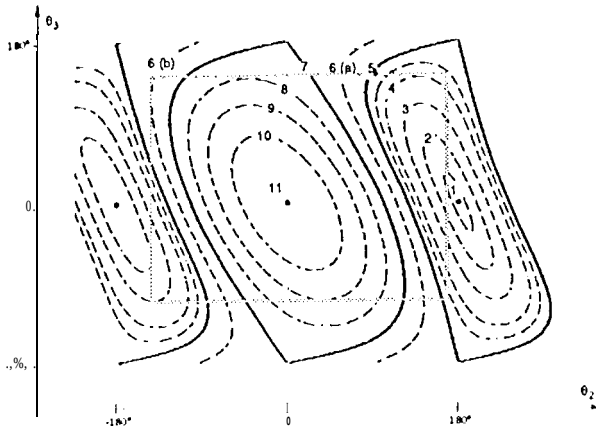

Figure 4: Self- Motion Manifold samples.

Nodes represent bundles and contain reference to the corresponding self-motion manifold topology. Some nodes are clustered to represent the collection of bundles premapped fro In a given w-sheet. Edges represent the transition from one bundle to the next through a co-regular surface. This graph provides concise and valuable information to assist a global planner in designing path strategies.

The interior singularities are easily identified as the intersection of two curves. The first singularity is given by $(\theta_2, \theta_3) = (1SO^\circ, 180^\circ)$ and corresponds to the polar radius $\rho = 5$. The second singularity is given by $(0, 180^\circ)$ with $p = 7$. The boundary singularities are marked for reference only, since they play only a marginal role in the current analysis. They are given by $(180^\circ, O)$, $p = 1$ and $(0, 0)$, $\rho = 11$.

Figure 6 focuses on the vicinity of the 2 interior singularities, showing how the neighboring manifolds converge to develop the hyperbolic pattern. Each self-r,)otioIL curve is labelled with the corresponding polar radius and reference to the bundle they belong to.

4 Joint Limits

The global behavior of redundant manipulators is drastically affected by joint limits.

Revolute joint space primitives without limits are modeled as circles, since a 360° rotation restores its initial configuration. Generalizing, a n-DOF revolute-jointed manipulator has its configuration space modeled as a n-torus.

Modeling a revolute joint with limits is in a way simpler, because it can be viewed as an interval rather than a circle. The

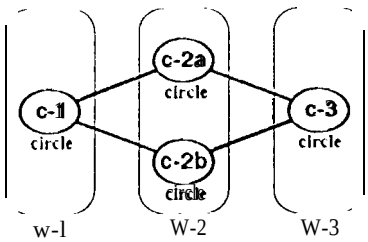

Figure 5: Connectivity graph for unbounded joints.

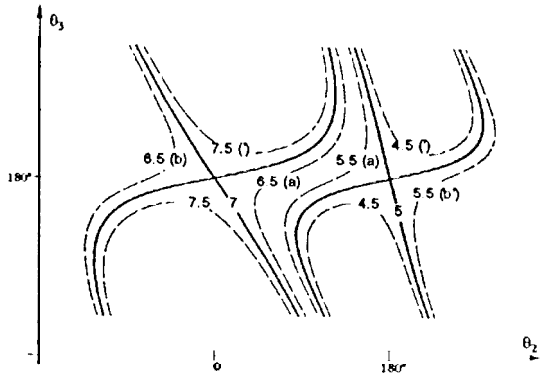

Figure 6: Self-Motion Manifolds near the Interior Singularities.

entire configuration space of limited revolute joints can be modeled as a n-I) hypercube rather than a n-torus. On the other hand, the consequences to the self-rnotion topologies are rather complex, as we address in this section.

If several but limited rotations are allowed at any joint, the issue of multiple solutions must be carefully analyzed. For an unbounded joint, a 360° rotation produces essentially the same solution. However, if tbe joint range is bounded, those solutions must be treated as different because their locations in the con figuration space with respect to the limits arc different. A planar 2-DOF revolute manipulator has in general 2 solutions for unbounded joints, but if troth joints arc bounded to two revolutions each, the number of distinct solutions becomes S.

Interms of the number of distinct solutions, a limitless joint behaves as a joint limited to a single revolution. From th at point on, for every rotary joint that doubles its range, the number of solutions is doubled as well.

The presence of joint limits has also a significant impact on the topology of self-motion manifolds. When the joint limit crosses the interior of a c-bundle, the k-homotopy within that bundle is disrupted and new k-homotopy classes emerge. New co-regular surfaces are created, splitting the original trundle into separate regions, each associated to a different k-homotopy class.

4.1 Example (cont.)

We described in section *3.1* the self-motion manifold topologies for the planar manipulator without joint limits. If we consider

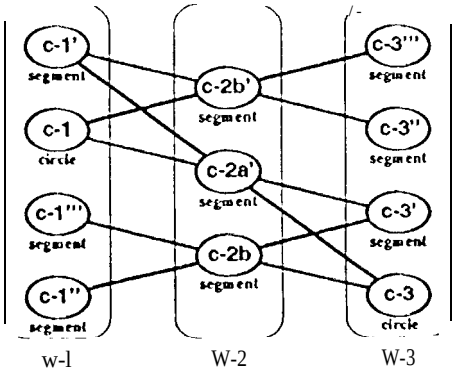

Figure 7: Connectivity Graph for $\theta_2, \theta_3 \in [-180^\circ, 360^\circ]$.

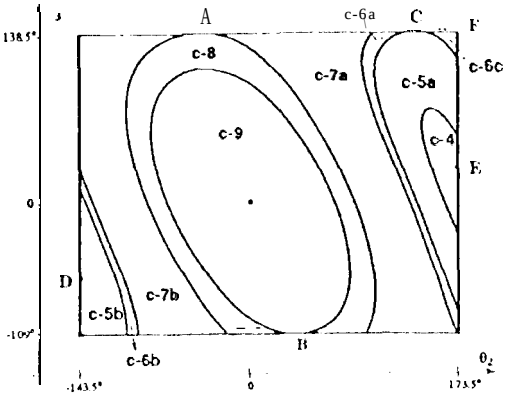

Figure 8: C-Bundles for θ_2, θ_3 as in eq. 6 .

joints 2 and 3 both limited to the interval [- lSO°, 360°] in Figure 3, we can see that self-rootion manifolds premapped from a position in w-1 become diffeomorphic to a circle (bundle c-1) and 3 segments (bundles c-1 ', c-1", c- 1" '). Analogously, the k-homotopy class of w-3 will consist of manifolds diffeomorphic to a circle and 3 segments. The w-2 sheet will be premapped to 3 c-bundles forming a k-homotopy class of manifolds diffeomorphic to 3 segments. Figure 7 shows the corresponding connectivity graph.

We introduce at this point the following constraints:

$$\begin{aligned} 143.5° < 02 < 173.5° \\ -109° < 03 < 13s.5° \end{aligned} \qquad (6)$$

For simplicity, without being unrealistic, joint 1 is unlimited in this example.

Figures 8 and 9 show the effect such joint limits produce in the configuration and work space topologies. The c-3 bundle (Figure 3) is cut twice by the limits of θ_3, generating 3 different sub-bundles. The innermost bundle, c-9, corresponds to the class of self.rl]otio]l manifolds not affected by the joint limits, continuing to be diffeomorphic to a circle. C-8 is cut once and the manifolds become segments.

The third region is cut twice and the premap becomes a pair of segments. Notice, however, that this third pair of manifolds becomes k-homotopic to the manifolds in the next pair of bundles (c-2a and c-2h in Figure 3) and we can merge those regions to obtain c-7a and c-7b. Notice also that the original co-regular surface where $\rho = 7$ has been removed in this process. This is due to the fact that the singularity which was used to generate that surface no longer belongs to the configuration space.

By the same token, the inner border of w-7 shifts from $p = 5$ to $p = 4.5$, where another factor comes into play. Due to the upper limit of θ_2, a third bundle is formed and the premap of a point in w-6 is diffeomorphic to 3 segments. In w-5 we have a pair of segments and in w-4 there is only one segment. The work space inner boundary was changed from $p = 1$ to $\rho = 1.2$.

Figure 10 shows the corresponding connectivity graph.

In order to assist in the visualization of these phenomena, we have included in Figure 4 a rectangle corresponding to the joint limits of this example and all manifolds involved at their extended shape.

5 The Scrni-Singularity

Section 4 described the impact of joint limits on the topology of self-lllotion manifolds. New c.o-regular surfaces are created and in this section we address the reasoning behind the appearance of those surfaces.

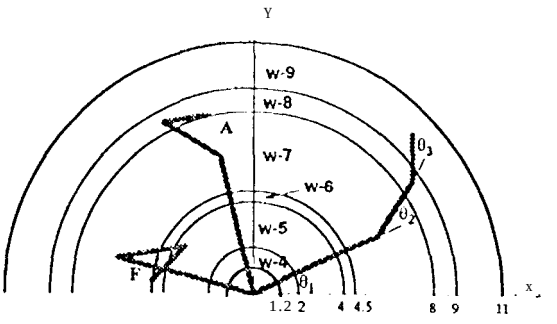

Figure 9: W-Sheets for 01,03 as in eq. 6

A standard co regular surface is pivoted by a manifold of singular configurations (cq. 3). In those singularities, the jacobian matrix loses its full rank and therefore velocities in a certain work space direction can not be generated. In the planar manipulator example, it rncans that all three columns of the 2 x 3 jacobian matrix arc linearly dependent (aligned) and the infeasible direction is orthogonal to those vectors. Notice that the singularity is bidirectional, i.e. if a certain velocity v is infeasible, so is - U.

$$J = [j_1\ j_2\ \cdots j_n] \qquad (-/)$$

The new co-regular surfaces are also pivoted by singularities, but the description of those singularities is more involved. The velocity domain of a joint at its limit is unidirectional, and so becomes the space spanned by the coI responding jacobian column. If the remaining joints do not generate a full rank map, the corresponding configuration is in semi-singularity) meaning that a certain velocity v is feasible but - u is not.

At a standard singularity, the range space shrinks from a hy - perspace to a hyperplane. At a semi-singularity, the range space becomes a semi-hyperspace. This conclusion can also be used to determine the shape of manipulability ellipsoids. This type of singularity produces a semi-ellipsoid.

The same line of reasoning can be made for the case where a semi-singularity occurs at the intersection of two or more joint limits. Being at the joint limit is therefore rrot a sufficient condition for the occurrence of a semi-singularity. It is required that the manipulator becomes singular (or at least semi-singular in case of multiple joint limits) without the contribution of the joint at its limit. Notice the fundamental difference in this respect between redundant and non-redundant manipulators. For non-redundant manipulators, every configuration with at least one joint at its limit is automatically semi-singular because the remaining joints can not restore full rank.

The ncw co-regular surfaces described in section 4 arc pivoted by semi-singularities which are mapped to the interior of the work space. Those semi-singularities which do not generate co-regular surfaces actually determine the ncw boundary of the work space, as we discuss in the next section.

5.1 Example (cont.)

In this section wc will describe the serni-singularities encountered in Figure 8.

There arc 6 semi-singularities in the example given by eq. 6, which are labelled A to F in Figure 8. Semi-singularities A, B and C occur at the joint 3 limits and configuration A is displayed in Figure 9. Notice that the cnd-effecter is aligned with link 1 and

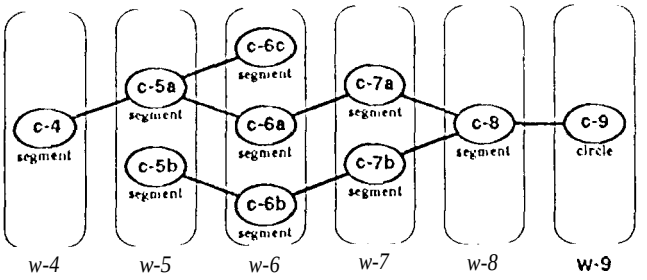

Figure 10: Connectivity Graph for $0_{2},03$ as in eq. 6

therefore both joints 1 and 2 generate end-effector velocities tangent to the circle ρ = S. Joint 3 can not fold itself any further and the.rcfolc the end-effector cannot enter into the w-7 sheet. nut the opposite direction is feasible and the arm is capable of moving the end-effector into w-8 at this configuration. Analytically we have:

$$\dot{\theta}_3 \leq 0, \det([j_1\ j_2]) = 0. \quad (8)$$

The same situation happens at configurations B and C. Notice that if the joint 3 limits were symmetric with respect to θ_3 = O, the semi-singularities A and B would belong to the same co-regular surface and the c-S bundle would disappear. Notice also that semi-singular i tics are easily recognizable in the configuration space. as points where the self-motion manifolds are tangent to the joint limit sui face. In fact, this semi-singularity property provides a method to search and identify semi-singularities along the joint limit surfaces.

The semi-singular ities D and E occur at the joint 2 limits but they are different in nature from the 3 previous ones. Point D generates a co-regular surface but it is itself not geometrically connected to it. This is duc to the fact that the self-rnotion manifold associated to D is tangent from the outside of the joint range. Point D still pivots a co-regular surface because the self-rnotiol, manifold generates a branch inside the configuration range, separating c-4 from c-5a.

Point E is also part of a self-rrlotior, manifold which is tangent to the joint limit from the outside, but it did not generate a co-regular surface. This is due to the fact that it corresponds to the new inner boundary of the work space and, as such, does not have the separating effect that interior singularities do.

The last semi-si ngularity, F, occurs at the intersection of two joint limits. The self-nlotion manifold corresponding to F is tangent at a corner and tbc configuration is also displayed in Figure 9. It is semi-singular because both jacobian columns subjected to the joint limit constraints are pointing into w-6 and therefore it is not possible to move the end-effector into w-7. The remaining 3 corners of the configuration space are not semi-singularities because one vector points inwards while the other points outward and therefore the configuration is still full rank.

Notice that semi-singularity F (and the entire c-6c bundle for that matter) corresponds to a configuration where links 1 and 3 overlap. If we arc to avoid that, wc must add this constraint to eq. 6, removing c-6c from the joint range. As it happens *in* general, the removal of a singularity from the configuration space is followed by the disappearance of the corresponding co-regular surface. In this case, removing c-6c causes the merging of w-6 with w-7 in the work spacc and c-6a with c-7a, c-6b with c-7b in the configuration space.

Table 1: Denavit-Hartenberg parameters for the AAI Arm.

i	α_i	d_i	α_i	joint_offset	joint range for θ_i
1	0	d_1	'90"	0	θ_1 unlimited ""
2	0	0	90°	180°	-105° < $\theta_2 \leq$ 105°
3	0	d_3	90°	180°	--165° $\leq \theta_3 \leq$ 165°
4	0	0	90°	lsO°	--105°<04<105°
5	0	d_5	-90°	90°	--165° $\leq \theta_5 \leq$ 165°
6	0	0	90°	90°	- 10 2° $\leq \theta_6 \leq$ 131°
7	0	0	90°	–90°	-130°<07<22"
s	0	d_8	0°	1 so"	θ_8 unlimited

6 Case Study: The A A I Arm

In this section we will apply the concepts presented in this paper to the 8-degree-of-frecdoln manipulator, called the AA I Arm.

The Denavit-Hartenberg parameters and the joint limit constraints for the AA I Arm arc show n in Table 1. Figure 11 shows the Arm and its work space.

A parameterized inverse kinematics for this manipulator is readily available, as well as tbc symbolic inverse jacobian [7].

The manipulator is naturally decomposable into two sub-arms serially connected.

The upper part is a redundant spherical wrist, responsible for the orientation of the end-effector. The lower part is primarily responsible for positioning, but the orientation of the end-effector is not invariant with respect to the self-rrlotion of the lower part. In other words, the self-motion of the upper part dots not require any counteraction from the lower part, but the lower part self-motion must in general be compensated by the upper part in 01 dcr to preserve the end-effector position and orientation.

We will describe the AA I Arm self-motion in two sections. The first section addresses the positioning self-lllotiorl due to the lower part. The orientation self-nlotion duc to the upper part in addressed in the second section.

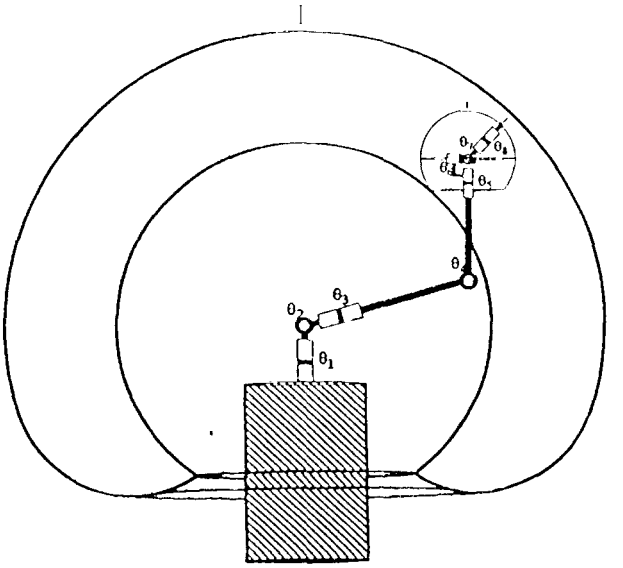

Figure 11: The AAI Arm and its work space.

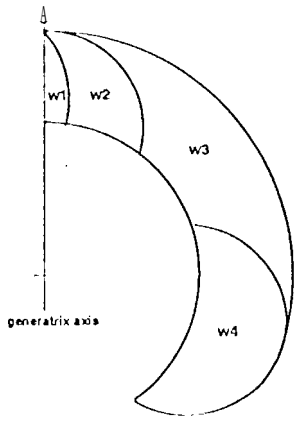

Figure 2: W-sheets for the lower part of the AAI Arm.

6.1 Positioning Self-Motion

The lower part of the AAI Arm contains four joints. The original design includes joint limits for the first joint as well, but in this paper we will consider joint 1 without limits in order to allow the visualization of co-regular surfaces in 3-D.

Based on this simplification, the 3-D work space is represented by its 2-D cylinder generatrix, as in Figure 12. In other words, the complete work space is obtained by a rotational sweep of the generatrix about the vertical axis, which coincides with the joint 1 axis. This procedure allows us to represent the kinematic map as from a 3-dimensional configuration Space $(\theta_2, \theta_3, \theta_4)$ to a 2-dimensional work space (the generatrix).

Figure 13 shows the c-bundles and co-regular surfaces obtained for all singularities and semi-singularities of the lower part. Thin lines are self-motion representatives along a co-regular surface. The thicker lines represent some of the semi-singularities encountered in this case. Figure 14 shows the corresponding connectivity graph.

The singularities arc:

1. The lines given by $\theta_2 = 0, \theta_3 = 90°$ and $\theta_2 = 0, \theta_3 = -90°$
2. The plane given by $\theta_4 = 0$.

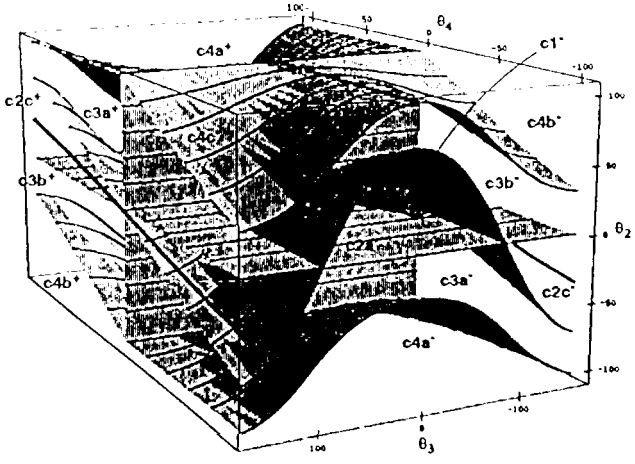

Figure 13: C-Bundles for the lower part of the AA] Arm.

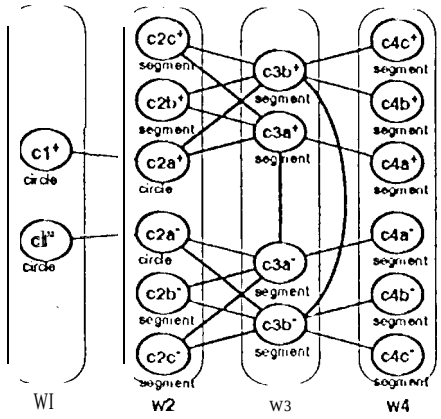

Figure 14: Connectivity Graph for the lower part of the AA I Arm.

The sclli-singularities are:

1. The lines given by $\theta_2 = 105°, \theta_3 = 0, \theta_4 < 0$ and $\theta_2 = -103", \theta_3 = 0, \theta_4 > 0$.
2. One curve in each of the joint limit surfaces given by $\theta_3 = 165°$ and $\theta_3 = -165°$ (no analytic description is available).
3. The planes given try $\theta_4 = 105°$ and $\theta_4 = -105°$.

We mentioned in the introduction section that boundary singularities do not generate co-regular surfaces because they do not separate between reachable regions in the work space. In order to separate a m-dimensional region we need a constraint of dimension at least $m - 1$ (a point separates a line, a line separates a plane, a plane separates a 3-J) region, etc). A jacobian surface is orthogonal to the singular direction and is usually of dimension $m - 1$, considering that only one degree of freedom is lost. The addition of self motion to those singularities produce surfaces in the configuration space of dimension $m - 1 + r = n - 1$, where r- is the degree of redundancy, and as such they can separate the n-dimensional configuration] space. By this simple dimensional analysis, we conclude that r admissible null space spanning vectors arc needed in order to produce the separating effect.

Boundary singularities (singularities occurring at the boundary of the work space) arc unescapable by nature, i.e. no self motion is capable of restoring full rank [2]. In most cases, the null space spanning vectors at boundary singularities arc unadmissible, i.e. there is no self-nlotion at such configurations and the inverse map is just a point (or a set of points due to symmetry). The result is a surface of dimension $m - 1$ embedded in a n-dimensional space. This surface can not sqm.rate the configuration space, by the same reason that a point can not separate a plane.

This phenomenon is easily visualized at the examples in the previous sections, where a boundary singularity is premapped to a point in the configuration space, unlike the premap of interior singularities, which arc curves.

However, there are cases where a null space vector may be admissible at a boundary singularity. For instance, if we have a positional manipulator and a rotary joint with its axis intersecting the end-effector at its boundary, the null space vector due to that joint velocity is admissible. This case study is an example of that. At the outer boundary ($\theta_4 = 0$), the joint 3 axis intersects the end-

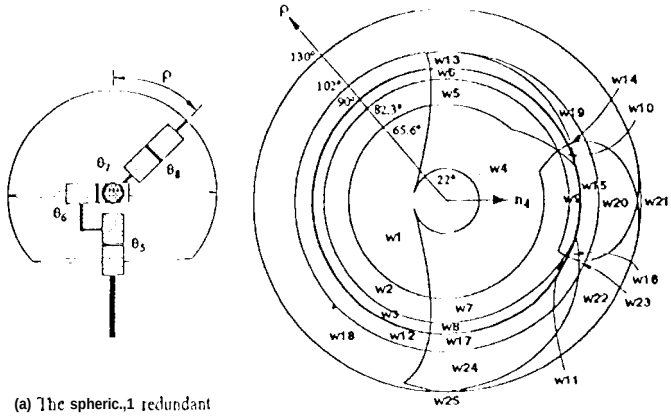

(a) The spheric.,1 redundant manipulator.

(b) Work space sheets for the upper part

Figure 15: The Spherical Redundant Manipulator and its work space representation.

effector. The manifold of those singular configurations is a plane rather than a line. Since those singularities are unescapable, the co-regular surface is the very singularity manifold: $CS = S$.

A boundary surface connects to a single w-sheet instead of two. Therefore, a co-regular surface due to a boundary singularity manifold can only separate between bundles of the same w-sheet. The graph in Figure 14 shows two connections between different bundles from the premap of w3. Those connections are produced by the $\theta_4 = 0$ plane.

The work space boundary semi-singularities given by $\theta_4 = \pm 105°$ also contain admissible null space vectors and therefore produce co-regular surfaces. However, no additional information is carried out by those two planes because they represent the work space boundary at the configuration space boundary.

6.2 Orientation Self-hfc)tioll

The upper part of the AA I Arm also consists of four joints, but

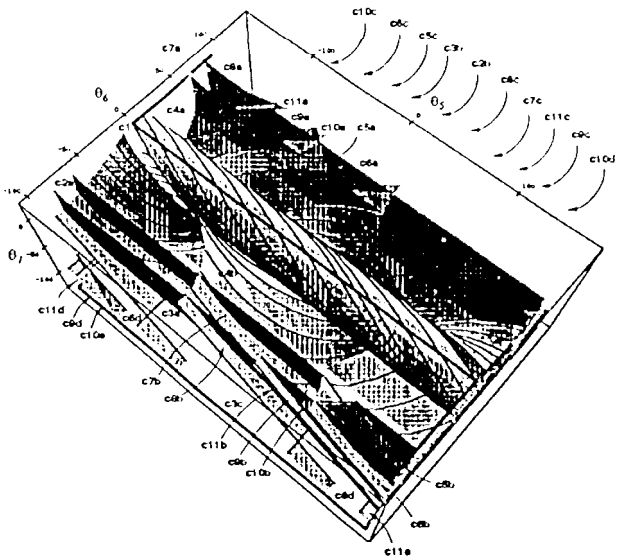

Figure 16: ~-bundles for the upper part: $0 < \rho < 90°$.

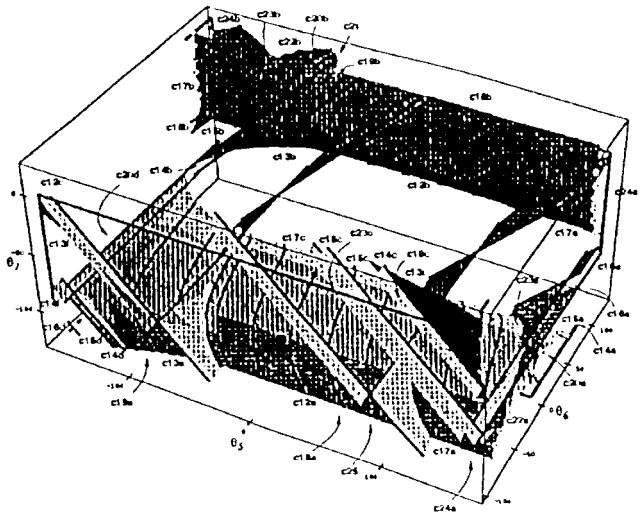

Figure 17: C-bundles for the upper part: $90° < p < 130°$

in this case our manifold map is complete because joint 8 is unlimited try design. It is therefore sufficient to describe the direction of the approaching vector, again a 3-D to 2-D map. The direction of the approaching vector is represented by a point on the surface of a sphere (Figure 15).

In order to visualize the work space in two dimensions, we apply a topological deformation of the sphere, utilizing the natural opening at the bottom produced by the joint limits (Figure 15). Analytically, the redundant forward map just described is represented by the following set of equations in polar coordinates:

$$p = \cos^{-1}(c_6 c_7) \tag{9}$$

$$\phi = \mathrm{Atan2}(c_5 s_6 c_7 + s_5 s_7, c_5 s_7 - s_5 s_6 c_7). \tag{10}$$

The polar radius p represents the angle between the approaching vector a_8 and the vertical axis of the upper part, a_4. The polar angle ϕ represents the angle between the projection of a_8 onto the plane perpendicular to a_4 and the normal vector n_4. Notice that Frame 4 is the end-effector frame for the lower part as well as the hasc frame for the upper part. Equation 10 may be factorized to $\theta_5 + \tan^{-1}(s_6 c_7 / s_7)$ for the appropriate arctangent, which demonstrates the direct relationship between θ_5 and the polar angle ϕ.

Figure 15 shows the jacobian surfaces as they separate the work space into 25 w-sheets. The jacobian surface given by $\rho = 90°$ is highlighted because it is due to the only interior singularity of this arm and it separates the configuration space into 6 regions, named $R1$ to $R6$ as in Figure 18. Since this surface divides the work space into two regions, it is convenient to analyze each of those regions separately. Figure 16 shows the c-bundles premapped from the inner circle $0 < p < 90°$ into regions $R1$, $R2$ and $R3$. Figure 17 shows the c-bundles premapped from the outer ring $90° < p < 130°$ into regions $R4$, $R5$ and $R6$. Finally, Figure 18 shows the connectivity graphs for the inner and outer part as well as the connections from one to the other through the co-regular surface given by $p = 90°$. For simplicity, the topology of the node is not included, In this cam, all manifolds are segments. Furthermore, the nodes do not contain the full name of the bundle because of lack of space. The full name can be inferred from the corresponding w-sheet it premaps to.

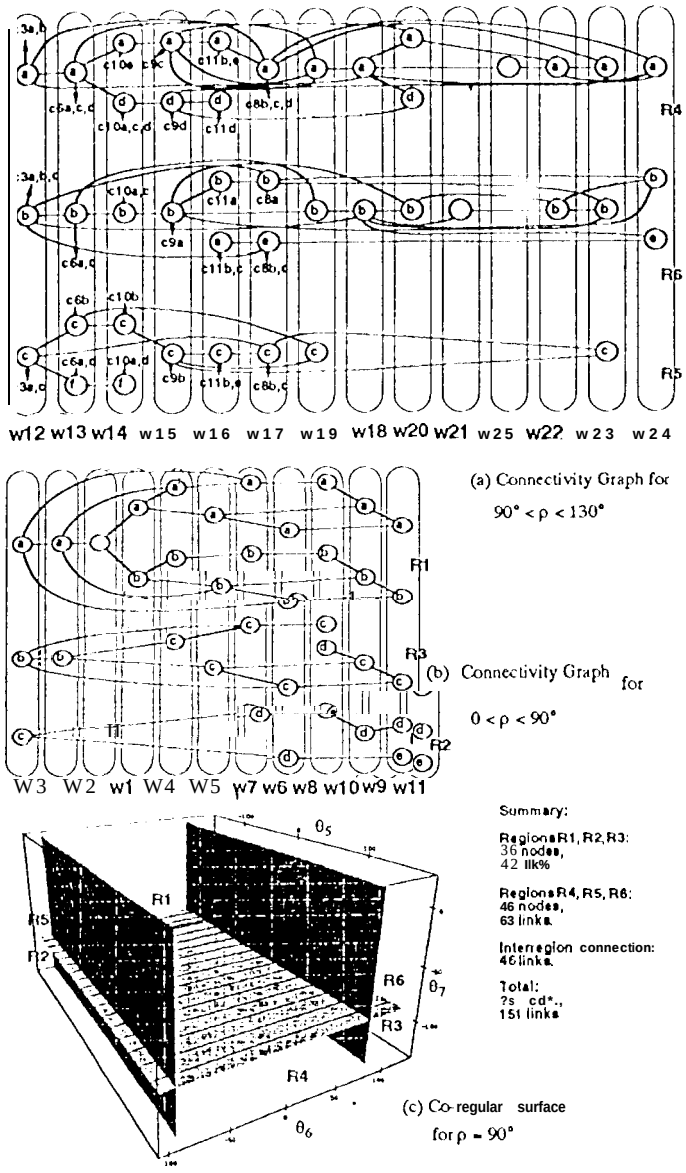

Figure 1S: Connectivity Graphs for the upper part.

For example, the top leftmost node is labelled "a" and it is a premap of w12, therefore its full name is c12a.

Note the complexity of this case, as compared to the same example without joint limits. In the later case, the connectivity graph would consist of only 4 nodes and 4 links. This is a concrete example of how the presence of joint limits can drastically increase the complexity of manifold maps. Given the fact that most manipulator designs incorporate such constraints, it is imperative that we understand the effects those constraints produce and design methods to analyze and explore it. This paper is aimed at this very point. Based on the properties of semi-singularities, the entire process can be automated and even be utilized as a design parameter to optimize the global performance of redundant manipulators.

7 Summary and Conclusion

As the manipulator crosses a co-regular surface, the self-motion manifolds are ruptured like branches of a hyperbola passing through the center. This effect justifies the appearance of different k-homotopy classes and ultimately determines the connectivity of configurations across neighboring bundles. A connectivity graph can be generated and the information contained in it can be used at the top level of a global planner to determine strategies to optimally satisfy a given set of constraints.

The introduction of joint limits reshapes the entire topology of self-motion manifolds and creates new types of singularities which are unidirectional in nature. They were called semi-singularities because the range space in the absence of a direction becomes a semi-space.

As the dimension of the system increases, the topology effects of joint limits become even more severe, justifying the need for an adequate framework and basic principles to be used for the analysis of redundant manipulators. In this paper, the framework of manifold maps has been refined and basic principles were introduced, such as semi-singularities and their corresponding co-regular surfaces.

A case study presents preliminary results on the application of the concepts discussed in this paper to a spatial redundant manipulator.

We are currently pursuing the implementation of a global redundancy resolution and planner algorithm which will benefit from the discoveries presented in this paper.

Acknowledgement: The research described in this paper was carried out in part by the Jet Propulsion Laboratory, California Institute of Technology, under a contract with the National Aeronautics and Space Administration, and in part by the University of Southern California.

References

[1] D. P. Martin, J. Baillieul and J. M. Hollerbach, "Resolution of Kinematic Redundancy Using Optimization Techniques," IEEE Transactions on Robotics and Automation, Vol. 5, No. 4, pp. 529-533, August 1989.

[2] N. S. Bedrossian, "Classification of Singular Configurations for Redundant Manipulators, " Proc. IEEE Int. Conf. on Robotics and Automation, pp. 818- S23, 1990.

[3] J. W. Burdick, "On the Inverse Kinematics of Redundant Manipulators: Characterization of the Self-Motion Manifolds," Proc. IEEE Int. Conf. on Robotics and Automation, pp. 261--270, 1989.

[4] R. Dubey and J. Y. Luh, "Redundant Robot Control for Higher Flexibility," Proc. IEEE Int. Conf. on Robotics and Automation, pp. 10661072, 1987.

[5] A. Ghosal and B. Roth, "A h'cw Approach for Kinematic Resolution of Redundancy," The International Journal of Robotics Research, Vol. 7, No. 2, pp 22-35, March/April 1988.

[6] C. Lück and S. Lee, "Self-hfotion Topology for Redundant Manipulators with Joint Limits", Proc. IEEE Int. Conf. on Robotics and Automation, Atlanta, 1993.

[7] S. Lee and A. K. Bejczy, "Redundant Arm Kinematic Control Based on Parameterization ," Proc. IEEE Int. Conf. on Robotics and Automation, pp. 458-465, 1991.

[8] W. S. Massey, Algebraic Topology: Ar, Introduction, Springer-Verlag, New York, 1967.

[9] G. Strang, Linear Algebra and its Applications, Academic Press, Sccorrd Edition, 1980.

[10] C. W. Wampler, 11, "Inverse Kinematic Functions for Redundant Manipulators," Proc. IEEE Int. Conf. on Robotics and Automation, pp. 610-617, 1987.

[11] Ph. Wenger, "A New General Formalism for 'the Kinematic Analysis of all Nonredundant Manipulators)" Proc. IEEE Int. Conf. on Robotics and Automation, pp. 442-447, 1992.